GPU-Based Real-Time Approximation of the Ablation Zone for Radiofrequency Ablation

Christian Rieder, Tim Kröger, Christian Schumann, and Horst K. Hahn
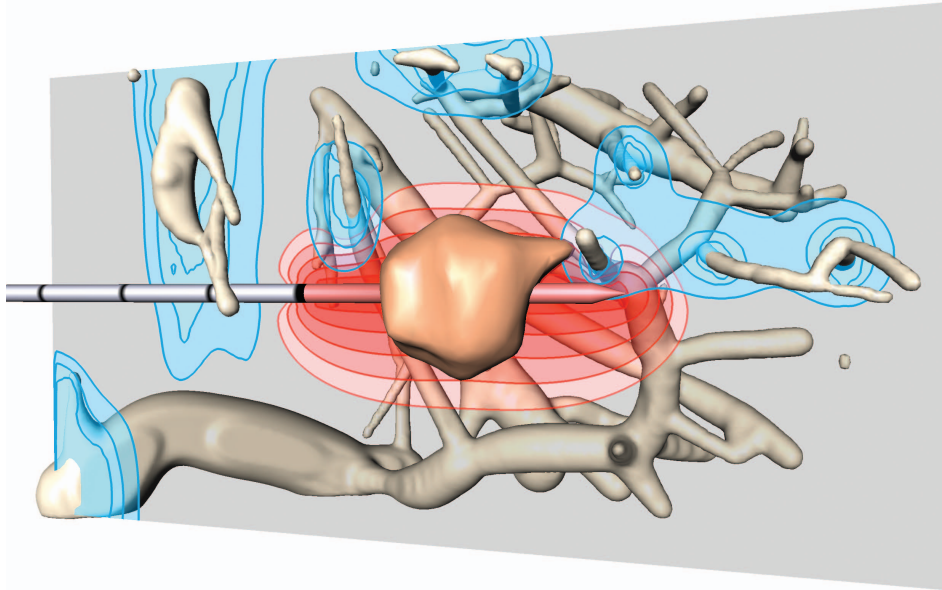
Fig. 1. The RF applicator is placed into the tumor, and the corresponding approximative ablation zone incorporating the heat-sink effect is displayed as red isolines. The blue isolines represent the thermal cooling of the blood vessels around the lesion.

Abstract—Percutaneous radiofrequency ablation (RFA) is becoming a standard minimally invasive clinical procedure for the treatment of liver tumors. However, planning the applicator placement such that the malignant tissue is completely destroyed, is a demanding task that requires considerable experience. In this work, we present a fast GPU-based real-time approximation of the ablation zone incorporating the cooling effect of liver vessels. Weighted distance fields of varying RF applicator types are derived from complex numerical simulations to allow a fast estimation of the ablation zone. Furthermore, the heat-sink effect of the cooling blood flow close to the applicator's electrode is estimated by means of a preprocessed thermal equilibrium representation of the liver parenchyma and blood vessels. Utilizing the graphics card, the weighted distance field incorporating the cooling blood flow is calculated using a modular shader framework, which facilitates the real-time visualization of the ablation zone in projected slice views and in volume rendering. The proposed methods are integrated in our software assistant prototype for planning RFA therapy. The software allows the physician to interactively place virtual RF applicator models. The real-time visualization of the corresponding approximated ablation zone facilitates interactive evaluation of the tumor coverage in order to optimize the applicator's placement such that all cancer cells are destroyed by the ablation.

Index Terms—Radiofrequency ablation, ablation zone visualization, distance field, volume rendering, GPU, interaction.

---- ◆ ----

1 INTRODUCTION

Image-guided ablation therapies using thermal energy, particularly radiofrequency ablation (RFA), have been developed as a minimally invasive alternative to surgical resection of liver tumors [7]. Due to its common technical procedure, low complication rate, and low cost, RFA has become a widely used alternative in the clinical routine. The principle of the RFA therapy is the placement of RF applicator electrodes into the tumor. Subsequently, a high-frequency electric field is induced that causes localized heating and leads to a coagulative necrosis as a result of cell destruction. The success of the therapy depends on the choice of an appropriate applicator type and the placement of its electrodes into the lesion to achieve complete destruction of cancer cells with respect to the heat-sink effect of the cooling blood vessels.

In this work we present a novel approach to approximate the ablation zone (thermal necrosis) in order to support the physician in interactive planning of radiofrequency ablation. Contributions of our work include:

- Proposal of a model based on weighted distance fields to approximate the ablation zone, incorporating heat-sink effects of the blood vessels. The weighted distance fields are retrieved

- *Christian Rieder and Christian Schumann are with Fraunhofer MEVIS, E-mail: {christian.rieder | christian.schumann}@mevis.fraunhofer.de.*
- *Tim Kröger is with CeVis, University of Bremen, E-mail: tim.kroeger@cevis.uni-bremen.de.*
- *Horst K. Hahn is with Fraunhofer MEVIS and with Jacobs University Bremen, E-mail: horst.hahn@mevis.fraunhofer.de.*

from complex numerical simulations that take the bio-physical effects into account. To consider the cooling blood vessels, we calculate the thermal equilibrium of the vasculature in a preprocessing step. The final ablation zone is the result of a heuristic combination of both fields.

- Integration of the approximation model into a clinical software assistant. We utilize the graphics hardware to calculate and visualize the approximated ablation zone in real-time in both, 2D and 3D. The underlying dynamic shader framework allows the user to perform interactions such as parameter adjustments or intuitive placement of multiple RF applicators with corresponding ablation zones.

- Assessment of the value of our method. We compare the results of our method with complex numerical simulations. Furthermore, a discussion of our method with interventional physicians in an informal expert study completes our contribution.

2 MEDICAL BACKGROUND

The principle of RFA therapy is to percutaneously insert RF applicators (through the skin) into the target organ (cf. Fig. 2) and destroy all cancer cells of the target lesion by means of thermal necrosis as a result of an alternating electric field that oscillates in the high-frequency range (200 - 1.200 kHz). Coagulative necrosis is a result of irreversible protein denaturation of the destroyed cells, which is achieved by local resistive heating of the tissue to cytotoxic temperatures (50°- 100°C) in the entire target volume for at least 4-6 minutes. Typically, the target volume includes a safety margin of approximately 10 mm around the tumor to handle uncertainties and microscopic clusters of cancer cells around the visible tumor tissue. Besides the choice of applicator type, the induced energy and the ablation time affect the size of the resulting coagulation. Additionally, blood vessels in the vicinity of the RF applicator can lead to a cooling of the heat distribution, the so-called *heat-sink effect*, which locally decreases the size of the coagulative necrosis.

Generally, image-guided RFA therapy can be divided into three clinical steps:

- Planning: Before the intervention, pre-interventional images are used to plan the optimal trajectory and the optimal electrode position to facilitate a complete ablation of the tumor. Thereby, important risk structures such as large vessels, ribs, and lungs, are taken into account.

- Intervention: During the intervention, the RF applicator is monitored by means of peri-interventional image guidance to support placement of the electrode into the planned target area and to control the ablation progress (as well as parameters such as the induced energy). MR thermometry is sometimes used to monitor the resulting heat distribution.

- Assessment: After the intervention, pre- and post-interventional images are compared to evaluate the treatment success, i.e., identify whether the tumor could be completely ablated or not.

Typical RF applicators are needle-shaped and have radii of 0.9 - 1.0 mm and overall lengths between 100 - 250 mm, depending on the type and manufacturer. Various types of electrodes are available. They are either monopolar, i.e., only one electric pole is on the applicator and the other is placed on the body using a plate electrode (see Fig. 3), or bipolar, i.e., both electric poles are on the applicator (see Fig. 4). Simple applicator designs feature electrodes that are located directly on the needle and cover an area which typically has a length of 10 to 40 mm (the so-called *active area*). More complicated electrode configurations like umbrella-shaped monopolar electrodes have been developed to allow for necrosis of different shape and larger size. Applicators are connected to an external power generator which allows the physician to control the induced energy.

RFA is clinically indicated as a minimally invasive therapy if the tumor is of less than 40 mm in diameter, multiple lesions are scattered

in the liver, or a surgical resection is contraindicated, e.g., due to the general constitution of the patient [18]. A recent study [4] reports, that the initial treatment of secondary liver tumors larger than 25 mm has shown a high local recurrence rate because of inaccurately placed applicators or the inability to produce a predictable, large coagulation volume. Another study states that the local recurrence rates after RFA for tumors with an intentional margin of 0 mm and 10 mm are 14.5% and 6.5%, respectively [17].

Clinically, the estimation of the ablation zone and the resulting determination of an optimal applicator position before the intervention is a critical task to ensure the success of the therapy. In a typical procedure in the clinical routine, the physician utilizes measurement tools to determine an optimal probe trajectory to the target volume and mentally estimates the resulting ablation zone. In this work, we focus on software-assisted RFA planning and aim to support the physician by utilizing the visualization of ablation zones. In most planning applications, the ablation zones are typically described as ellipsoids around the RF applicator electrodes [3, 32, 25], which are specified for homogeneous tissue by the applicator manufacturers. However, this estimation of the ablation zone is questionable if patient-specific planning of the intervention is desired. Due to the presence of cooling blood vessels in the vicinity of the RF applicator, the coagulation size may be decreased and the tumor incompletely ablated [17]. To overcome this issue, numerical simulations based on FEM have been developed to allow an accurate estimation of the ablation zone to incorporate heat-sink effects [10] and integrated into prototypical software assistants. Although the results of these methods are helpful to understand physical effects, they are not suited for the clinical routine because of long calculation time. Hence, in this work, we present a real-time approximation of the estimated necrosis that supports the interactive planning of optimal applicator electrode placement in the tumor with respect to the heat-sink effects of the blood vessels.
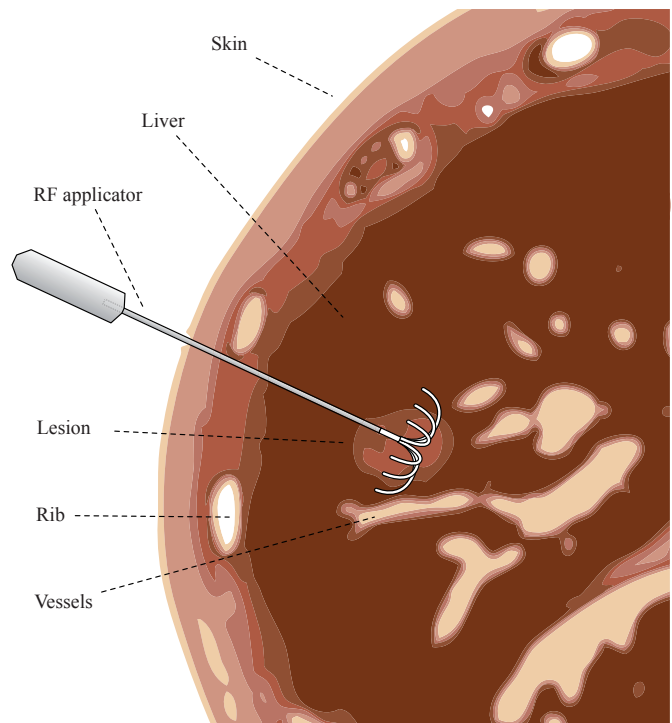

Fig. 2. An umbrella-shaped monopolar applicator is percutaneously placed in the liver. The electrode is positioned in the tumor and the prongs are spread for ablation.

3 RELATED WORK

Butz et al. [3] present a software tool based on *3D Slicer* for preoperative simulation and planning of tumor ablation, including radiofre-

quency, laser, and cryoablation. Arbitrary virtual ablation devices can be added to the 3D scene and are visualized using surface models. Ablation zones are modeled utilizing simple geometry: for cryoablation, ellipsoids are used to model the frozen zones at the tip of each cryoneedle, and for radiofrequency, spherical models represent the ablation zones.

Another software application for planning RFA treatment is described by Villard et al. [32], who focus on planning support for ablation of hepatic tumors. Liver, blood vessels, pathologies, and surrounding organs are automatically segmented and visualized by means of surface rendering. Also, virtual RF applicator models with idealized ellipsoidal ablation zones are available. To model the heat-sink effect, the ablation zone models are deformed in real-time by moving their vertices according to the proximity of large surrounding liver vessels [33]. Technically, a morphological opening operation is applied to the vessel mask to eliminate small vessels ($\varnothing < 2\text{-}3$ mm) as a preprocessing step. Using further dilations, a deformation zone is calculated to define the amount of vertex translation. Besides the limitation of the possible vertex deformation of the ellipsoid, this approach is purely heuristic, so that the relation of the applied deformation to the biophysical heat-sink effect of the blood vessels during RFA is unclear.

Littmann et al. [13] present a software system for in-situ laser-induced thermotherapy (LITT) ablations in oncologic liver surgery. LITT applicators are represented as surface models and can be visualized in the familiar 2D slice views as well as in a 3D surface rendering. Also, intrahepatic structures can be segmented to simulate the ablation zone. The heat transport incorporating heat-sink effects of surrounding vessels within the liver tissue is calculated by means of a time-consuming finite differences method.

McCreedy et al. [14] present a registration, segmentation, and fusion tool for RFA treatment planning. In this application, the liver, hepatic vasculature, and lesions can be semi-automatically segmented. Virtual RF applicator models of various manufacturers, and the corresponding expected ablation zones are rendered as surface models, in 3D only. However, the segmented vasculature is not taken into account for the estimation of the expected ablation zones, which are modeled as simple ellipsoids.

Weihusen et al. [35] describe a workflow-oriented software platform for image-guided RFA. Virtual applicator models of different manufactures can be superimposed onto the 2D slice images. Furthermore, tumor lesions and vascular structures can be segmented using semi-automatic methods. The extracted vessels are utilized for the numerical simulation of the ablation zone incorporating the cooling effects of nearby vessels. The ablation zone resulting from the numerical simulation is visualized in 2D viewers as an overlay and also in a volume rendering as a surface model. In a subsequent work [25], the expected ellipsoidal ablation zones, as specified by the manufacturers, are also included as an alternative to the time-consuming numerical simulation. To allow an intuitive placement of the probes, tumor regions outside the ablation zone are emphasized.

Zhai et al. [36] present a preoperative surgery planning method for percutaneous microwave ablation. The microwave ablation zone is simulated utilizing an iterative GPU calculation. The ablation zone is visualized along with the microwave applicator in the 2D slice views and in 3D as a surface model combined with the anatomical volume rendering. Computation times of less than 2 seconds are reported for the simulation, whereas the typical rendering time reaches 20 FPS using an Nvidia GeForce 8800GTS graphics card.

Kröger et al. [11] present an approximation of the numerical forward simulation. In this approach, the patient-specific ablation zone is parameterized by a large number of reference configurations, which are precomputed and stored in a lookup table. During placement of the applicator electrode, the patient-specific ablation zone is reconstructed from the lookup table under consideration of the Euclidean distance from the electrode to the blood vessels and its radii, allowing for interactive frame rates. This approach is further integrated into a medical application, allowing for slice-based rendering of the ablation zone [23]. The major drawbacks of this method are, that the basic shape of the ablation zone consists of the union of spheres along the

points of the electrode and the critical assumption of an independent cooling effect per vessel segment.

Trovato et al. [31] include an approximation of combined multiple ablation zones into their semi-automatic RFA planning system. Although the visualization method is not described in detail, it can be assumed that some kind of implicit blending is used. However, heat-sink effects are not taken into account.

In this work, we propose a novel model to approximate the ablation zone which incorporates heat-sink effects of the blood vessels. In contrast to the discussed related work, the model is based on weighted distance fields retrieved from complex numerical simulations taking the biophysical effects into account. Furthermore, the approximated ablation zone is calculated on the graphics hardware, allowing for interactive frame rates.

More references and theoretic details have been compiled in an overview article by Berjano [2]. A comprehensive review of computer-assisted planning of liver tumor ablation is presented in the work of Schumann et al. [28].

4 APPROXIMATION OF THE ABLATION ZONE

In the literature, ablation zones of different applicator types are often estimated as simple ellipsoids, as specified by the manufacturers, in homogeneous tissue. However, in practice, the simple ellipsoid is merely a rough estimation of the ablation zone, particularly in the case of umbrella-shaped electrodes or multiple bipolar applicators. In our work, we estimate the ablation zone in real-time with weighted distance fields [9] incorporating electrode geometry. The distance fields are retrieved from results of complex numerical simulations in homogenous tissue, which allow a more realistic representation of the ablation zone than as simple ellipsoids.

4.1 Description of the Ablation Zone

4.1.1 Monopolar RF Applicator

The principle of monopolar RFA is to create a closed-loop circuit consisting of the monopolar electrode, a large dispersive electrode (ground pad), and the patient. The monopolar electrode and the ground pad are connected to the generator. An alternating electric field is induced through the electrodes, whereby the patient acts as a resistor. A typical monopolar applicator consists of a simple needle electrode or an array of umbrella-shaped prongs. During placement of the electrode, the prongs are folded inside the applicator. Once the electrode is in position, the array is spread to the umbrella shape, and radiofrequency ablation may begin. Typically, after a first ablation cycle, the prongs are folded up, the electrode is pulled back (10-15 mm), and the prongs are rolled off for further ablation. Fig. 3 illustrates an umbrella-shaped monopolar RF applicator.
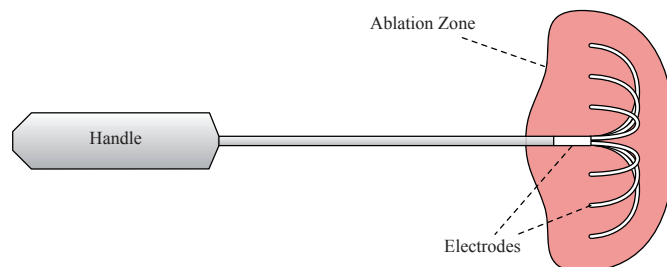

Fig. 3. Illustration of a monopolar RF applicator with a deployed array of umbrella-shaped electrode prongs and typical ablation zone.

4.1.2 Bipolar RF Applicator

In contrast to the monopolar applicator, the bipolar applicator consists of two electrodes, separated by an isolator (cf. Fig. 4). Because the electric energy is supplied between those two electrodes, the tissue is heated around both electrodes. Thus, a large dispersive electrode is not required for a closed circuit. To increase the ablation zone, up to

three bipolar applicators can be placed close to each other and simultaneously connected to a single generator. In such a multi-applicator setting, the electrical field is induced in a round-robin fashion between all possible combinations, resulting in an extended ablation zone. An additional technique to increase the ablation zone is to internally cool the electrodes. Direct heating around the electrode is reduced to prevent the tissue from overheating and charring, which leads to an interruption of the RF circuit.
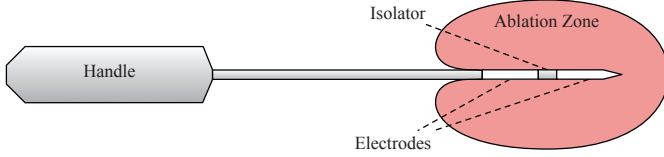

Fig. 4. Illustration of a bipolar RF applicator with corresponding ablation zone. The two electrodes are separated by an isolator. The applicator shaft is internally cooled resulting in the typical shape of the ablation zone in the direction of the handle.

4.2   A Mathematical Model

A mathematical model for RF ablation essentially consists of two partial differential equations:

$$\nabla \cdot (\sigma \nabla \phi) = 0, \tag{1}$$
$$\rho c \partial_t T - \nabla \cdot (\lambda \nabla T) + \nu(T - T_{\text{body}}) = q. \tag{2}$$

The first equation models the electric potential ϕ, which can be assumed to be quasi-static. Here, σ denotes the electric conductivity. The second equation models the distribution of the temperature T, where ρ, c, λ, and ν denote material parameters (that is, the density, the heat capacity, the thermal conductivity, and the relative blood flow rate). Further, T_{body} is the human body temperature (a constant), and q is the heat source induced by the electric current flow, it is given by

$$q(\boldsymbol{x}) = \alpha p(\boldsymbol{x}), \qquad p(\boldsymbol{x}) = \sigma |\nabla \phi(\boldsymbol{x})|^2, \qquad \alpha = \alpha(\|p\|_{L^1}), \tag{3}$$

where α is a one-parameter, scalar-valued function that models the nonlinear behavior of the electric generator due to changes of the tissue impedance. All material parameters are functions of the temperature T. In particular, σ depends on T, which in connection with (3) makes (1), (2) become a coupled system.

Equations (1), (2), and (3) compose a generalization of the so-called *thermistor problem*, well-known in the literature. The thermistor problem is recovered for $\alpha = \text{const}$ and $\nu = 0$. The term $\nu(T - T_{\text{body}})$ models the heat-sink effect due to the small blood vessels (invisible in pre-interventional imaging), by which the tissue is assumed to be pervaded. Equation (2) is called the *bio-heat transfer equation* [20, 5].

Both differential equations are considered on a computational domain Ω around the applicator electrodes which is chosen large enough such that effects outside the domain can be safely ignored. The area covered by the applicator is cut out of the domain for (1), and also for (2) if an internally cooled applicator is considered. The area covered by large blood vessels (visible in pre-interventional imaging) is cut out of the domain for (2). Both equations are supplemented by boundary conditions on the boundary Γ_{out} of the domain as well as on the boundaries of those parts that have been cut out of the domain. The boundary conditions are as follows:

$$\phi(\boldsymbol{x}) = \pm 1, \qquad\qquad \boldsymbol{x} \in \Gamma_{\pm}, \tag{4a}$$
$$n(\boldsymbol{x}) \cdot \nabla \phi(\boldsymbol{x}) = 0, \qquad\qquad \boldsymbol{x} \in \Gamma_{\text{iso}}, \tag{4b}$$
$$n(\boldsymbol{x}) \cdot \nabla \phi(\boldsymbol{x}) = \frac{n(\boldsymbol{x}) \cdot (\boldsymbol{s} - \boldsymbol{x})}{|\boldsymbol{s} - \boldsymbol{x}|^2} \phi(\boldsymbol{x}), \qquad \boldsymbol{x} \in \Gamma_{\text{out}}, \tag{4c}$$
$$T(t, \boldsymbol{x}) = T_{\text{body}}, \qquad\qquad \boldsymbol{x} \in \Gamma_{\pm} \cup \Gamma_{\text{iso}}, \tag{4d}$$
$$T(t, \boldsymbol{x}) = T_{\text{body}}, \qquad\qquad \boldsymbol{x} \in \Gamma_{\text{ves}}, \tag{4e}$$
$$n(\boldsymbol{x}) \cdot \nabla T(t, \boldsymbol{x}) = 0, \qquad\qquad \boldsymbol{x} \in \Gamma_{\text{out}}. \tag{4f}$$

Here, $\Gamma_{\pm}$, Γ_{iso}, and Γ_{ves} denote the boundary of those parts of the domain covered by the electrodes, the electrically isolating parts of the applicator, and the large blood vessels. In (4c), $\boldsymbol{s}$ denotes the centroid of the applicator's active zone. Equation (4d) models the applicator cooling and is removed from the system in case of an uncooled applicator. Equation (4e) models the heat-sink effect due to the large blood vessels, which are assumed to not heat up considerably [11]. The equation for the temperature is also supplemented by the initial condition

$$T(t, \boldsymbol{x}) = T_{\text{body}}, \qquad\qquad t = 0. \tag{5}$$

The coupled system is discretized using finite elements in space and a backward Euler scheme in time. Details can be inferred from a previous publication [10].

In order to determine the area of coagulated tissue, the tissue damage $D = D(t, \boldsymbol{x})$ is computed using an Arrhenius law [1],

$$D(t, \boldsymbol{x}) = \int_0^t A \exp\left(\frac{-E}{RT(s, \boldsymbol{x})}\right) ds,$$

where R is the universal gas constant and A and E are tissue parameters. This law takes a temperature history into account. The area of destroyed tissue (coagulative necrosis mask) is then given by the set

$$I_{\text{sim}} = \{\boldsymbol{x} \in \Omega : D(t_{\max}, \boldsymbol{x}) \geq 1\},$$

where $t_{\max}$ denotes the total ablation time.

4.3   Approximation utilizing a Weighted Distance Field

The key idea of our contribution is the approximation of the necrosis mask I_{sim} by iso-thresholding a weighted distance transform. Let α be a positive, real parameter. On the computational domain excluding the area covered by the electrodes (that is, on $\Omega \setminus \overline{\Omega_{\pm}}$ where $\Omega\pm$ denotes the area covered by the electrodes), we define the weighted distance transform

$$f(\boldsymbol{x}) = \left(\frac{1}{|\Omega_{\pm}|} \int_{\overline{\Omega_{\pm}}} \frac{1}{|\boldsymbol{x} - \boldsymbol{y}|^{\alpha}} d\boldsymbol{y}\right)^{-1/\alpha}, \tag{6}$$

where for any measurable set $A \subset \Omega$, the notation $|A|$ denotes the three-dimensional Lebesgue measure (i.e., the volume) of A. By setting $f(\boldsymbol{x}) = 0$ on $\overline{\Omega_{\pm}}$, we have defined f everywhere on Ω. Using this function and another positive parameter d, we define our approximation $I_{\text{zone}}(d, \alpha)$ of the necrosis mask as the d-iso-threshold of f, that is

$$I_{\text{zone}}(d, \alpha) = \{\boldsymbol{x} \in \Omega : f(\boldsymbol{x}) \leq d\}.$$

In practice, to evaluate f, we use a uniform sampling of all electrodes and approximate the integral by an appropriate weighted sum. That is, if there are n electrodes and each electrode is sampled with m points $\boldsymbol{s}_{ij}$, $i = 1, \ldots, n$, $j = 1, \ldots, m$, we approximate f by

$$\tilde{f}(\boldsymbol{x}) = \left(\sum_{i=1}^{m} \sum_{j=1}^{n} \frac{1}{m \cdot |\boldsymbol{x} - \boldsymbol{s}_{ij}|^{\alpha}}\right)^{-1/\alpha}. \tag{7}$$

Besides the length and shape of the electrodes, the parameters d and α affect the size and shape of the ablation zone $I_{\text{zone}}(d, \alpha)$. Namely, the value of α influences the shape of the mask, and d influences its size. That is, for $\alpha \to 0$, the limit shape is a ball of diameter d, whereas for $\alpha \to \infty$, the limit shape is the union of all balls of diameter d around all electrode points (cf. Fig. 5).

For any given applicator and given ablation parameters (such as electric power and ablation time), we determine the appropriate parameter values d and α in order to minimize the volumetric difference between reference and approximated ablation zone. That is, we compute the reference mask I_{sim} using the simulation described in Section 4.2 and then solve the optimization problem

$$|(I_{\text{sim}} \setminus I_{\text{zone}}(d, \alpha)) \cup (I_{\text{zone}}(d, \alpha) \setminus I_{\text{sim}})| \overset{!}{\to} \min$$
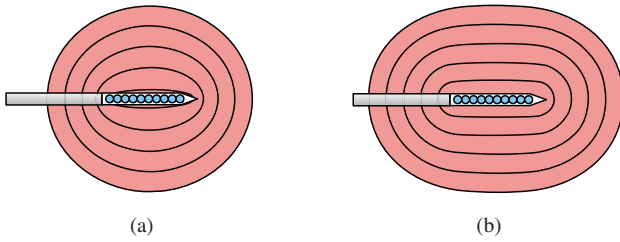
(a)   (b)

Fig. 5. Two images of the distance field illustrate the influence of the weight α for fixed-distance iso values. In (a), a low $\alpha = 1$ results in a spherical shape, i.e., the distance to the electrode's center sample is measured. In (b), a high $\alpha = 25$ results in a shape which is given by a union of balls, i.e., the minimal distance to each sample point is measured.

using the simplex optimization method [19].

We compute the values of d and α for a large variety of ablation configurations, including varying electrode lengths, ablation time, and generator power. The values are stored in a database. This method is also applicable to umbrella-shaped monopolar electrodes.

5   MODELING THE HEAT-SINK EFFECTS

So far, we presented our method to estimate the ablation zone in homogenous tissue. However, if the patient individual anatomy is taken into account, the assumption of homogeneous tissue leads to overestimated ablation zones. The major effect that decreases the size of the ablation zone is the cooling effect of large blood vessels. To take the heat-sink effect into account, we calculate an additional distance field from the vessels and estimate the amount of cooling which affects the thermal heating of the electrodes and thus deforms the shape of the ablation zone.

5.1   Description of the Heat-Sink Effect

Besides the physical electrode and physiologic tissue material parameters, the heat-sink effect particularly depends on the vessel diameter and the distance between vessel surface and applicator electrode. A possible method is to calculate a modified Euclidean distance transform of the vessels, where the vessel's diameters are taken into account. However, the drawback of this method is that only the minimal distance from a sample to the nearest vessel is encoded. That is, combined cooling effects of two nearby vessels cannot be described by this method. If multiple vessels are located close together, the coagulation zone suffers from spurious sharp edges, see Fig. 6.

5.2   Estimating the Thermal Equilibrium of the Vasculature

To overcome this issue, a simplified numerical simulation is used to estimate the space-dependent heat-sink effect independent of the applicator settings. This is done by solving (2) (together with the boundary conditions (4e) and (4f)) where q is now assumed to be a (spatially and temporally) constant heat source. By this, the equation becomes decoupled from (1). Also, the material parameters λ and ν are assumed to be constant, which makes the corresponding steady-state equation

$$-\nabla \cdot (\lambda \nabla T) + \nu(T - T_{\text{body}}) = q \qquad (8)$$

a linear elliptic partial differential equation, the finite element approximation of which can easily be solved in one step. Due to the linearity, the value of the constant heat source q is irrelevant because it simply acts as a scaling parameter.

Technically, the solution of the steady-state equation described above is performed using the full numerical simulation described in Section 4.2, where no applicator is placed, but rather the value T_{body} is replaced with $T_{\text{warm}} := T_{\text{body}} + q/\nu$ in (2) (but not in (4e) and (5)), and only one very large time step (step size 1000 seconds) is computed. Because the value of q can be chosen arbitrarily, the same holds for
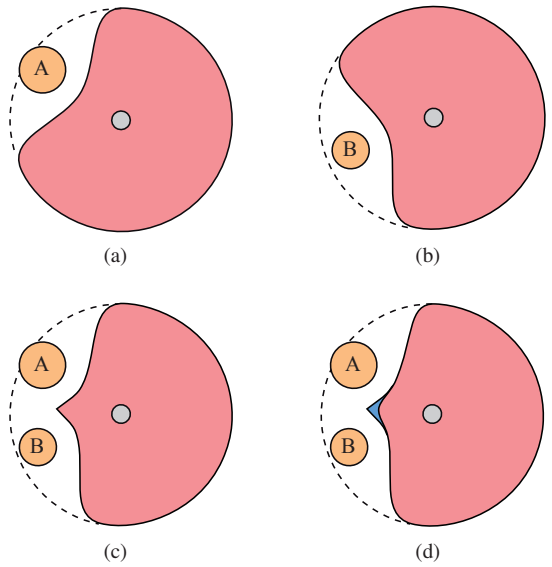

(a)   (b)

(c)   (d)

Fig. 6. In figure (a), the presence of vessel A leads to a deformation of the ablation zone according to the heat-sink effect. A similar situation is illustrated in (b). If an independent cooling effect is assumed, the final ablation zone is achieved by the intersection of both ablation zones (c). In contrast, if both vessels jointly cool the heat field, the heat-sink appears more smoothly (cf. blue peak), similar to the results of numerical simulations (d).

T_{warm}. After the solving (8), we define the function g as the normalized steady-state temperature by

$$g(\boldsymbol{x}) = 1 - \frac{T(\boldsymbol{x}) - T_{\text{body}}}{T_{\text{warm}} - T_{\text{body}}}. \qquad (9)$$

In our computation, we are use $T_{\text{warm}} = T_{\text{body}} + 10$, but because T_{warm} only acts as a scaling parameter in (8) and this scaling is canceled by (9), the function g is independent of the value of T_{warm}. Further, we have that $0 \leq g(\boldsymbol{x}) \leq 1$ for all $\boldsymbol{x}$, where $g(\boldsymbol{x}) = 1$ if and only if $\boldsymbol{x}$ is located inside a vessel, and $g(\boldsymbol{x}) = 0$ for all $\boldsymbol{x}$ if there are no vessels present. In particular, large values of g correspond to strong cooling and $g = 0$ corresponds to no cooling.

5.3   Deformation of the Ablation Zone

To estimate the heat-sink effect of the cooling vessels, we utilize the function g defined in the previous section and combine it with the weighted distance field of the ablation zone. Formally, we combine the two functions f and g using appropriate transition functions t_1 and t_2. Because the cooling only decreases the lesion size (rather than increasing it), it suffices to perform the additional computation on I_{zone} (where we now skip the parameters d and α in the notation). Because, by definition, $0 \leq f(\boldsymbol{x}) \leq d$ on I_{zone}, it is convenient to divide $f(\boldsymbol{x})$ by d before applying the transition function, because both transition functions then act on the same interval $[0, 1]$. Hence, we define the modified ablation zone by

$$I_{\text{cool}} = \left\{ \boldsymbol{x} \in I_{\text{zone}} : t_1(\tfrac{1}{d}f(\boldsymbol{x})) + t_2(g(\boldsymbol{x})) \leq t_1(1) + t_2(0) \right\}.$$

Note that the threshold has been chosen such that in the case of no vessels ($g(\boldsymbol{x}) = 0$ for all $\boldsymbol{x}$), we have $I_{\text{cool}} = I_{\text{zone}}$. In numerical experiments, we measured the distances from electrode to simulated necrosis mask and from a parallel aligned vessel mask to necrosis mask. After analyzing the distances for different spacing between vessel and electrode, it heuristically turned out that choosing the arcsin function for both t_1 and t_2 leads to good results. Hence, we have

$$I_{\text{cool}} = \left\{ \boldsymbol{x} \in I_{\text{zone}} : \arcsin(\tfrac{1}{d}f(\boldsymbol{x})) + \arcsin(g(\boldsymbol{x})) \leq \tfrac{\pi}{2} \right\}. \qquad (10)$$

In conclusion, we describe how we model the approximation of the ablation zone. By sampling the applicator's electrodes and calculation of a weighted distance field, the ablation zone can be fitted to the resulting necrosis mask of a complex numerical simulation. Heat-sink effects are estimated by solving the thermal equilibrium of the vasculature and the combination with the weighted distance field.

If, in addition, the applicator is internally cooled (cf. Sect. 4.1.2), this cooling can be taken into account in the same way as the vessel cooling. However, computation and usage of the combined function g for vessels and cooled applicator is not possible, because for varying applicator placements, the combined cooling mask would change. Real-time processing could no longer be achieved, because the computation of g involves the solution of a partial differential equation. However, we can compute a cooling field g_a for the cooled applicator *independently* of the cooling field g_v for the vessels in the same manner as described above (cf. Section 5.2). When the applicator is moved, the according affine transformations are performed to g_a, and the approximative ablation zone is then given by

$$I = \left\{ \boldsymbol{x} \in I_{\text{zone}} : \arcsin(\tfrac{1}{d} f(\boldsymbol{x})) + \arcsin(g_v(\boldsymbol{x})) + \arcsin(g_a(\boldsymbol{x})) \leq \tfrac{\pi}{2} \right\}.$$

Due to the rotational symmetry of the shaft, the function g_a is stored in a one-dimensional lookup table perpendicular to the shaft. Figure 7 illustrates the complete approximation model for a cooled bipolar applicator and a thermal field of the cooling vasculature.
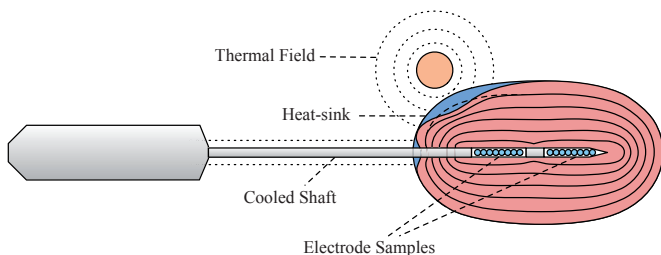

Fig. 7. Both electrodes of an internally cooled bipolar RF applicator are sampled. The corresponding weighted distance field is illustrated by isoline contours. The thermal fields of the blood vessels and the cooled applicator shaft decrease the ablation zone (blue areas).

6 APPLICATION

In comparable applications, the typical workflow is to load the patient data set, perform segmentation algorithms to classify structures of interest, and place virtual RF applicator models. Patient-independent ablation zones, such as ellipsoids, are available with the corresponding applicators, otherwise patient-specific numerical simulations have to be performed for a determined probe position. We follow this design regarding the needed preprocessing steps but enable the patient-dependent real-time visualization of approximated ablation zones.

6.1 Preprocessing

The first step is to load the patient data set. The tumor is segmented using a semi-automatic, morphology based region-growing algorithm [16] to determine the target volume for the ablation. For that, the user has to draw a stroke across the lesion for histogram analysis and seed point determination. The algorithm performs the binary segmentation within 1-3 seconds and has proven to be robust on different tumor entities and image noise. Furthermore, the vessels surrounding the tumor have to be extracted to calculate the thermal transport for the approximation of the ablation zone. For that, we utilize a Bayesian vessel extraction [37] algorithm which works locally in a region of interest (ROI). The algorithm typically runs less than two seconds to extract a vessel located in a ROI of roughly 64^3 voxels. The ROI is defined by a spatial position, determined by mouse-clicking into one vessel. Complex vessel trees may be manually composed by the user. Subsequently, the thermal equilibrium of the vasculature is estimated

using the vessel mask as image input as described in Section 5.2. Even though a complex PDE has to be solved, the numerical simulation calculates the thermal field in less than 5 seconds (for a ROI of the same size). Once the described preprocessing steps are performed, virtual applicator models can be added to the scene and corresponding ablation zones are visualized.

6.2 Calculation of the Ablation Zone

To calculate the ablation zone in real-time, we exploit the high performance of the graphics hardware. Technically, we make use of a recently presented modular shader framework [24] for both, 2D slice and volume rendering. For every RF applicator, the corresponding electrode is represented as a finite number of electrode samples. A shader function calculates whether each fragment's spatial position in world space is inside or outside of the ablation zone, by sampling the applicator's electrode. For that, equation (6) (or rather its approximation (7)) is evaluated taking the corresponding predefined distance d and weight α into account. Further parameters include the spatial position and the orientation of the RF applicator as well as parameters describing the electrode's geometry. Algorithm 1 illustrates the calculation of the weighted distance field per fragment. The final value is stored in a global data structure of the shader. To facilitate combined ablation zones from multi-applicator settings, the weighted distance field is calculated by sampling all active electrodes.

After calculating the weighted distance field, the cooling effect of the blood vessels is estimated. For all fragments classified as ablation zone, the cooling weight is fetched from the thermal field, represented as scalar volume, and the cooled ablation zone mask is calculated by evaluating (10). Subsequently, fragments which belong to the ablation zone, but are cooled under the temperature threshold are tagged as cooled ablation zone and cached in the data structure for later visualization.

---

input : electrode parameters, thermo field
output: ablation zone mask per fragment

$distance \leftarrow 0$;
for $electrode : e \in electrodes$ **do**
    $distance_e \leftarrow 0$;
    $sample_e \leftarrow (0,0,0)$;
    for $s \leftarrow 0$ **to** $electrode\ samples$ **do**
        $sample_s \leftarrow \texttt{calcSample}(s, params_e)$;
        $dist_s \leftarrow \texttt{distance}(sample_f, sample_s)$;
        $distance_e \leftarrow distance_e + \frac{1}{s_{max} pow(dist_s, \alpha)}$;
    end
    $distance \leftarrow distance + distance_e$;
end
$distance \leftarrow pow(distance^{-1}, \alpha^{-1})$;
$ablationZone \leftarrow \texttt{step}(distance, d)$;
$ablationZone \leftarrow \texttt{calcCooling}(distance, d, thermo field)$;

Algorithm 1: Calculation of the approximated ablation zone mask per fragment utilizing the weighted distance field and the thermal field of the blood vessels.

6.3 2D Slice Visualization

For planning of RFA, 2D slice renderings of volumetric data are commonly used in the clinical routine. Thus, we present visualization methods to overlay the ablation zone onto the anatomical image data such as the pre-interventional CT image. Although displaying of orthogonal projections is the clinical method of choice, few authors in the field of RFA planning focus on comprehensive 2D visualization [30] in contrast to 3D surface [27] or volume renderings [29]. To display the ablation zone, we present the following visualization methods:
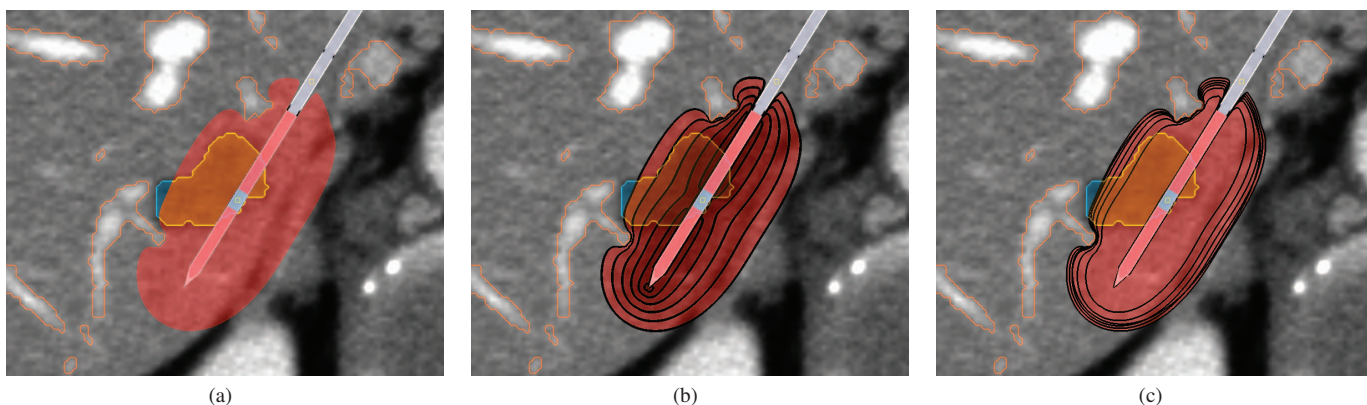
Fig. 8. Three projected slice visualizations of a bipolar RF applicator with corresponding approximated ablation zone (20 electrode samples, 30 watt generator power). In (a), the ablation zone is displayed as volumetric overlay. (b) Uniform isolines represent the topology of the weighted distance field. (c) Multi-parameter isoline visualization of 1, 2, 4, 8, and 16 minutes of ablation progress.

Volumetric overlay. The most common representation of image masks are volumetric overlays on top of anatomical images. Similarly, we visualize the approximated ablation zone as an overlay combined with the virtual applicator model. For every fragment classified as ablation zone, a specified color and alpha value is blended with the underlying anatomical image. Different color and alpha values may be assigned to fragments which are under-ablated due to the heat-sink effect, that is, fragments that belong to $I_{zone} \setminus I_{cool}$. Additionally, to emphasize tumor voxels which are not covered by the ablation zone, these voxels can be highlighted with a special color (cf. Figure 8 (a)). Technically, the cached values in the global data structure are directly mapped to fragment colors and alpha values, respectively.

Distance contours. Another visualization method to represent the ablation zone is the display of contours [15]. We utilize contours to draw isolines with uniform contour interval in order to emphasize the topology of the weighted distance field, particularly if the ablation zone is deformed due to the presence of blood vessels. The advantage of this method is that the visualized topology leads to an intuitive understanding of the involved heat-sink effects. For that, we calculate the weighted distance field in the 4-neighborhood of the current fragment. The contour for a specific distance value is extracted by detecting the edge from the neighborhood utilizing a dilatation operation. Multiple contours are drawn by taking varying distance values into account. Optionally, the isolines may be combined with the volumetric overlay, or different colors may be used for different isolines. Figure 8 (c) shows five uniform isolines of the distance field combined with the proposed overlay visualization.

Multi-parameter contours. Inspired by the uncertainty visualization of Praßni et al. [21], we propose a further contour visualization method to represent multiple parameters at the same time. Instead of drawing the contours at different distances to represent the topology, every contour is calculated from an independent weighted distance field. The parameterization of the multiple distance fields may be chosen according to the temporal progression or varying initial generator power of the numerical simulations. Thus, by drawing multiple contours together, the temporal progression of the coagulative necrosis with fixed generator power can be visualized. Analogously, multiple contours can also be utilized to visualize multiple ablation zones with varying generator power together (for a determined ablation duration). Technically, contours from the weighted distance field have to be calculated multiple times, taking varying parameters for the distance and the weight into account. Figure 8 (b) shows a multi-parameter isoline visualization. Five ablation durations of 1, 2, 4, 8, and 16 minutes are displayed together. The advantage of this method is that a simultaneous exploration of multiple ablation settings is possible in order to optimize the electrode placement.

6.4 3D Volume Visualization

In addition to the 2D slice visualization, we also combine the approximative ablation zone with a 3D volume rendering of the surrounding anatomy. The liver parenchyma is visualized in a transparent fashion to allow a clear view of the liver vessels, which are emphasized utilizing the automatic determination of an appropriate transfer function **??**. The benefit of the anatomical volume visualization is a fast recognition of potential risk structures such as the liver vessels, which have to be protected from harm, combined with the approximated ablation zone. Because physicians like surgeons or gastroenterologists are not as familiar with slice representations as radiologists, the volume rendering may be particularly helpful for them to intuitively recognize the spatial relations.

Technically, the ablation zone is calculated with the same shader function used for the 2D slice rendering, although the composition is differently parameterized according to the accumulation of the alpha values for volume rendering. Also, tumor voxels outside the ablation zone are emphasized by alternating colors. In order to represent internal structures such as the colored tumor, the ablation zone may be rendered in a transparent fashion. The drawback of the transparent rendering is that the shape of the ablation zone, and thus the constrictions due to the cooling vessel, can not be recognized due to missing shading information.

To emphasize the shape of the ablation zone, we utilize volume shading. The gradients required for the shading model are calculated on the fly using central differences [8] from the weighted distance field. Thus, the distance field also has to be calculated for the 6-neighborhood of every sample. To reduce the additional calculation time, the electrodes are downsampled up to one fifth of the original samples, resulting in a fourfold increase in speed. The resulting loss in shading quality is negligible. With downsampling, 15-16 fps are measured, rendering a region of interest of 110^3 voxels and an image resolution of 512×512 pixels on an ATI Radeon HD 5870 (40 fps without shading).

The advantage of the shaded ablation zone is the representation of the shape. In order to emphasize internal structures of the ablation zone (e.g., the tumor), we utilize boundary and silhouette enhancement [22]. In Figure 9 (a-c), the advantage of the enhancement is illustrated. In contrast to the simple rendering, the ablation zone and the surrounded lesion can be displayed together without loss of spatial information.

7 COMPARISION AND EVALUATION

7.1 Comparison with the Numerical Simulation

In order to estimate the accuracy of our approximation method, we compare the ablation zone with the coagulative necrosis mask from the numerical simulation in complex vascular situations, extracted
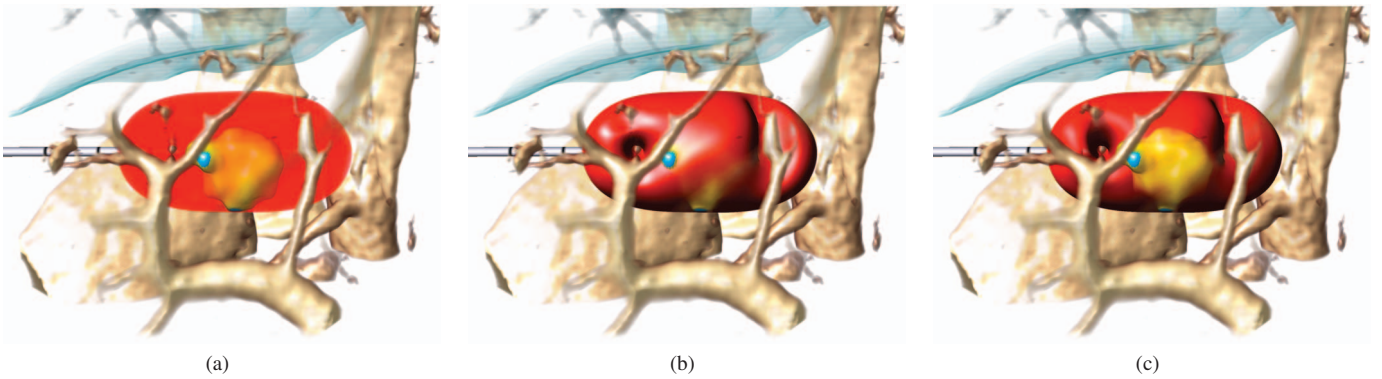
(a)   (b)   (c)

Fig. 9. Comparison of three volume visualization techniques of the approximated ablation zone. In (a), the ablation zone is rendered in a transparent fashion without shading, allowing the user to examine the tumor overlap. In (b) shading is enabled, which results in a clear representation of the the ablation zone's shape. In order to emphasize internal structures, boundary and silhouette enhancement is utilized (c).
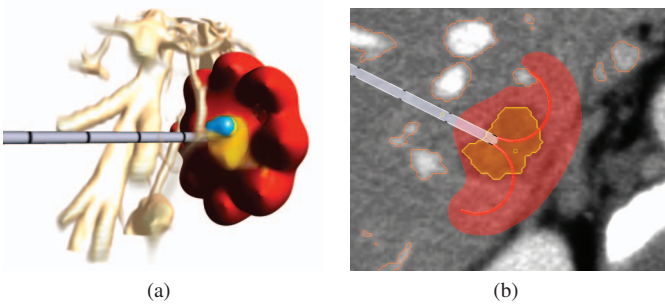

(a)   (b)

Fig. 10. Volume rendering of an umbrella-shaped monopolar RF applicator (a), and corresponding visualization of a single slice in plane with the applicator's shaft.
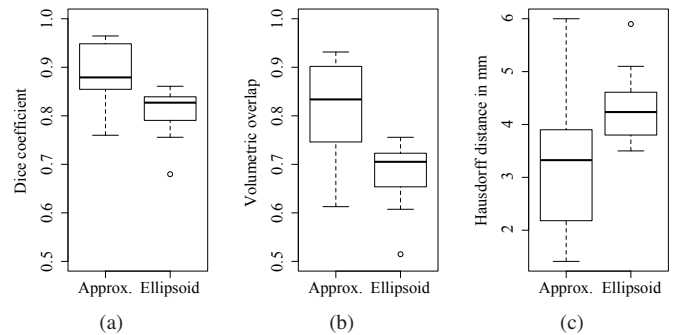

(a)   (b)   (c)

Fig. 11. (a) represents the averaged Dice coefficients from 10 simulation masks with corresponding approximation and ellipsoid masks, respectively. (b) shows the averaged volumetric overlap and (c) the Hausdorf distances in millimeter.

from 10 real data sets. In Figure 12, screen shots from two cases are presented. For each case we compare the simple ellipsoidal ablation zone, our approximation method, and the coagulative necrosis mask of a complex numerical simulation. For that, we reconstruct three-dimensional volume masks from slice representations of the ellipsoidal and approximated ablation zones. We chose the same image size as the computation domain of the numerical simulation. In all cases, bipolar applicators are placed (Celon ProSurge 150-T30^{TM} applicator, active zone length 30 mm, isolator length 3 mm, radius 0.9 mm). The coagulative necrosis masks are simulated for an ablation time of 16 minutes and a generator power of 30 W. The size of the computation domain is set to $65^3 mm$ (with a typical voxel size of around $0.7{\times}0.7{\times}1.0$ a resolution of approx. $92{\times}92{\times}65$ is defined), and the times for the calculation are between 30 and 50 minutes.

The resulting ablation zone masks are compared utilizing following metrics: volumetric overlap, Dice coefficient [6], and Hausdorff distance [26], i.e., the maximum surface distance of the masks in millimeter. The results are reported in Fig. 11. In the processed cases, the median Dice coefficient is 0.88 and the median volumetric overlap is 0.83, indicates a good correlation with the numerical simulation considering a speed up of the calculation time of up to 100,000. Dice coefficient and volumetric overlap after fitting the weighted distance field to the numerical simulation mask without consideration of the vessels are 0.99 and 0.97, respectively. Obviously, the greatest approximation error is introduced by incorporating the heat-sink effect of the blood vessels. Besides the promising results, we state that the validation of our numerical simulation is on active research [12, 34].

7.2 Expert Evaluation

Our method was presented to three experienced interventional physicians. They used our application to plan RF ablation of liver tumors on

real patient data sets. The clinicians stated the value of our method for planning RFA, particularly for situations in which large vessels are located in the vicinity of the target lesion or if multiple bipolar electrodes are placed around the lesion. In such situations, estimating the ablation zone using alternative methods such as mental suggestion or visualization of simple ellipsoids is challenging. Although mental planning of the RFA treatment by the physician is clinically the method of choice if no planning software is available, a high amount of expertise is required to take the patient-individual anatomy into account. Furthermore, the clinical experts explained that the value of the ellipsoid is questionable because heat-sink effects are not considered. In contrast, they stated that the approximated ablation zone looks much more realistic than the ellipsoid and that they would trust the in the visualization of the ablation zone. Principally, they would prefer the numerical simulation to visualize the expected ablation zone incorporating the cooling blood vessels. However, due to the high computational effort, which is too time-consuming for clinical use, the approximation was judged as a highly useful method for planning RFA. Also, the medical experts explained that our method is valuable to support inexperienced radiologists in interactively estimating the expected size and shape of the coagulative necrosis and thus find an optimal trajectory to the target volume under consideration of relevant risk structures.

8 RESULTS AND CONCLUSIONS

We presented a novel method to approximate the ablation zone of different RF applicator models. We utilized a weighted distance field, fitted to the coagulative necrosis mask retrieved from a numerical simulation under consideration of the biophysical heat transport. The
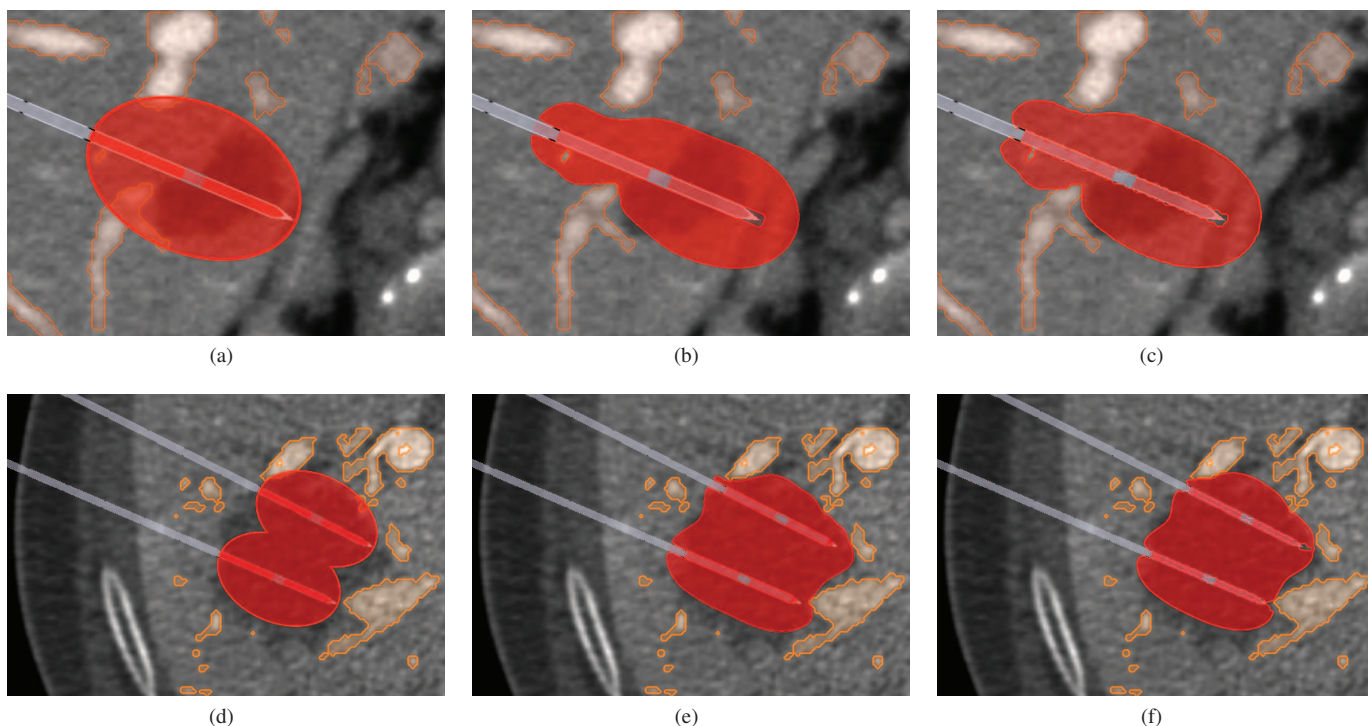
Fig. 12. Comparison of three methods estimating the ablation zone of bipolar RF applicators. In (a,d), the ablation zone is represented as simple ellipsoid. Heat-sink effects are not taken into account. Images (b,e) show the presented approximated ablation zone incorporating the cooling blood flow, and in (c,f) the coagulation mask of the numerical simulation is shown.

approximated ablation zone was combined with a thermal field, describing the heat transport of the vasculature in order to estimate the heat-sink effects of nearby blood vessels. Because the parameters describing the ablation zone are determined for homogeneous material parameters (i.e., patient independent) and the thermal field is calculated from the segmented vessel mask in a pre-processing step, the approximation of the resulting coagulative necrosis can be processed in real-time utilizing the GPU.

In contrast to similar work, we do not represent the ablation zone as a deformed ellipsoid. Instead, the ablation zone is approximated utilizing a weighted distance field, retrieved from a numerical simulation. In other work, the heat-sink effect is modeled by translating the vertices of the ellipsoid based on the proximity of large liver vessels. In our approach, we precalculate the thermal equilibrium of the vasculature and modify the ablation zone by combining the distance field and the thermal field based on heuristics. Another work presenting an approximation of the numerical simulation is the method by Kröger et al. [11]. In their approach, the ablation zone is parameterized by a large number of precalculated reference configurations, stored in a lookup table. A reference configuration is a simplified two-dimensional setting, where a vessel of infinite length is assumed to be parallel to the applicator's electrode. The look-up table has to be calculated under consideration of the Euclidean distance from the electrode to the blood vessels, the vessel radii, and the angle between the direction under consideration and the direction in which the vessel center is located. Thus, the major difference to our method is that the ablation zone is individually calculated for every vessel segment, resulting in an independent cooling effect (cf. Fig. 6). In both related works, the combined ablation zone of multiple RF applicators as well as the estimation of different electrode types, such as the umbrella-shaped applicator, are not reported. Furthermore, in our work we utilize advanced visualization techniques such as multi-parameter contour drawing or shaded volume rendering in 2D and 3D on interactive frame rates.

In the comparison of the approximation with the numerical simulation, we showed that similar ablation zone masks can be calculated, even in complex vascular situations, for both monopolar and bipolar electrodes and for multiple RF applicator configurations. Several limitations result from the substantial simplifications of our method. The most important limitation is that the approximation is only indirectly related to the biophysical principles. In situations where cooling vessels interrupt the thermal transport of the electrodes, the estimated shape of the ablation zone may be incorrect (cf. Hausdorff distance). However, the major benefit of our approach results from the real-time performance in both 2D and 3D, and the independence from the duration of the estimated ablation procedure. Visualizing a coagulative necrosis mask by solving numerical simulations results in high computation times ranging from a few minutes to several hours depending on the resolution of the computational domain (particularly the required high-resolution domain for representing umbrella-shaped electrodes), the ablation duration (5-30 minutes), and the chosen calculation precision. Furthermore, utilizing contour visualization, multiple parameters such as generator power or ablation duration can be represented together.

For future work, we plan to conduct a user study with medical experts to evaluate the clinical value of our method using real patient data. To estimate the benefit, RF applicators will be placed pre-interventionally and the ablation zone will be compared with the outcome of electrodes placed during the interventions. Furthermore, we also plan to integrate the approximation model into an automatic path proposal method for RF applicator placement. Besides other optimization constraints (e.g., the distance to risk structures), the performance of our method would facilitate a fast estimation of the tumor overlap in order to determine an optimal RF applicator placement, automatically.

REFERENCES

[1] S. Arrhenius. Über die Reaktionsgeschwindigkeit bei der Inversion von Rohrzucker durch Säuren. *Z. Phys. Chem*, 4:226–248, 1889.

[2] E. Berjano. Theoretical modeling for radiofrequency ablation: state-of-the-art and challenges for the future. *BioMed Eng OnLine*, 5(1):24, 2006.

[3] T. Butz, S. Warfield, K. Tuncali, S. Silverman, E. van Sonnenberg, F. Jolesz, and R. Kikinis. Pre- and intra-operative planning and simulation of percutaneous tumor ablation, Jan 2000.

[4] T. de Baere, A. Denys, B. J. Wood, N. Lassau, M. Kardache, V. Vilgrain, Y. Menu, and A. Roche. Radiofrequency liver ablation: experimental comparative study of water-cooled versus expandable systems. *AJR Am J Roentgenol*, 176(1):187–92, Jan 2001.

[5] P. Deuflhard and R. Hochmuth. Multiscale analysis of thermoregulation in the human microcascular system. *Mathematical Methods in the Applied Sciences*, 27(8):971–989, 2004.

[6] L. R. Dice. Measures of the Amount of Ecologic Association Between Species. *Ecology*, 26(3):297–302, 1945.

[7] S. Garrean, J. Hering, A. Saied, W. Helton, and N. Espat. Radiofrequency ablation of primary and metastatic liver tumors: a critical review of the literature. *Am J Surg*, 195:508–520, Jan 2008.

[8] M. Hadwiger, J. M. Kniss, C. Rezk-salama, D. Weiskopf, and K. Engel. *Real-Time Volume Graphics*. A. K. Peters, Ltd., Natick, MA, USA, 2006.

[9] M. Jones, J. Baerentzen, and M. Sramek. 3D Distance Fields: A Survey of Techniques and Applications. *Visualization and Computer Graphics, IEEE Transactions on*, 12(4):581 – 599, 2006.

[10] T. Kröger, I. Altrogge, T. Preusser, P. Pereira, D. Schmidt, A. Weihusen, and H. Peitgen. Numerical simulation of radio frequency ablation with state dependent material parameters in three space dimensions. *Proceedings of MICCAI*, 4191:380–388, 2006.

[11] T. Kröger, T. Pätz, I. Altrogge, A. Schenk, K. S. Lehmann, B. B. Frericks, J.-P. Ritz, H.-O. Peitgen, and T. Preusser. Fast estimation of the vascular cooling in rfa based on numerical simulation. *The Open Biomedical Engineering Journal*, pages 1–11, Mar 2009.

[12] K. Lehmann, J. Ritz, S. Valdeig, V. Knappe, A. Schenk, A. Weihusen, C. Rieder, C. Holmer, U. Zurbuchen, P. Hoffmann, H. Peitgen, H. Buhr, and B. Frericks. Ex situ quantification of the cooling effect of liver vessels on radiofrequency ablation. *Langenbeck's Archives of Surgery*, 394:475–481, 2009. 10.1007/s00423-009-0480-1.

[13] A. Littmann, A. Schenk, B. Preim, G. Prause, K. Lehmann, et al. Planning of anatomical resections and in situ ablations in oncologic liver surgery. *International Congress Series*, Jan 2003.

[14] E. McCreedy, R. Cheng, P. Hemler, A. Viswanathan, B. Wood, and M. McAuliffe. Radio frequency ablation registration, segmentation, and fusion tool. *Information Technology in Biomedicine, IEEE Transactions on*, 10(3):490 – 496, Jul 2006.

[15] J. L. Mitchell, C. Brennan, and D. Card. Real-time image-space outlining for non-photorealistic rendering. In *ACM SIGGRAPH 2002 conference abstracts and applications*, SIGGRAPH '02, pages 239–239, New York, NY, USA, 2002. ACM.

[16] J. Moltz, L. Bornemann, J.-M. Kuhnigk, V. Dicken, E. Peitgen, S. Meier, H. Bolte, M. Fabel, H.-C. Bauknecht, M. Hittinger, A. Kiessling, M. Pusken, and H.-O. Peitgen. Advanced Segmentation Techniques for Lung Nodules, Liver Metastases, and Enlarged Lymph Nodes in CT Scans. *Selected Topics in Signal Processing, IEEE Journal of*, 3(1):122–134, 2009.

[17] S. Mulier, Y. Ni, L. Frich, F. Burdio, A. L. Denys, J.-F. D. Wispelaere, B. Dupas, N. Habib, M. Hoey, M. C. Jansen, M. Lacrosse, R. Leveillee, Y. Miao, P. Mulier, D. Mutter, K. K. Ng, R. Santambrogio, D. Stippel, K. Tamaki, T. M. van Gulik, G. Marchal, and L. Michel. Experimental and Clinical Radiofrequency Ablation: Proposal for Standardized Description of Coagulation Size and Geometry. *Ann Surg Oncol*, 14(4):1381–96, Apr 2007.

[18] S. Mulier, Y. Ni, J. Jamart, L. Michel, G. Marchal, and T. Ruers. Radiofrequency Ablation Versus Resection for Resectable Colorectal Liver Metastases: Time for a Randomized Trial? *Ann Surg Oncol*, 15(1):144–57, Jan 2008.

[19] J. A. Nelder and R. Mead. A Simplex Method for Function Minimization. *The Computer Journal*, 7(4):308–313, Jan. 1965.

[20] H. H. Pennes. Analysis of tissue and arterial blood temperatures in a resting forearm. *J. Appl. Physiol.*, 1:93–122, 1948.

[21] J.-S. Praßni, T. Ropinski, and K. H. Hinrichs. Uncertainty-aware guided volume segmentation. *IEEE Transactions on Visualization and Computer Graphics (TVCG) (Vis Conference Issue)*, 16(6):1358–1365, nov, dec 2010.

[22] P. Rheingans and D. Ebert. Volume Illustration: Nonphotorealistic Rendering of Volume Models. *Visualization and Computer Graphics, IEEE Transactions on*, 7(3):253 – 264, Jul 2001.

[23] C. Rieder, I. Altrogge, T. Kröger, S. Zidowitz, and T. Preusser. Interactive Approximation of the Ablation Zone incorporating Heatsink Effects for Radiofrequency Ablation. *Proc. of CURAC*, pages 9–12, 2010.

[24] C. Rieder, S. Palmer, F. Link, and H. K. Hahn. A Shader Framework for Rapid Prototyping of GPU-Based Volume Rendering. *Computer Graphics Forum (Special Issue on Eurographics Symposium on Visualization)*, 30(3):1031–1040.

[25] C. Rieder, M. Schwier, A. Weihusen, S. Zidowitz, and H.-O. Peitgen. Visualization of risk structures for interactive planning of image guided radiofrequency ablation of liver tumors. *Proceedings of SPIE Medical Imaging*, Jan 2009.

[26] G. Rote. Computing the minimum hausdorff distance between two point sets on a line under translation. *Inf. Process. Lett.*, 38:123–127, May 1991.

[27] E. Samset, T. Mala, L. Aurdal, and I. Balasingham. Intra-operative visualisation of 3d temperature maps and 3d navigation during tissue cryoablation. *Computerized Medical Imaging and Graphics*, 29(6):499–505, 2005.

[28] C. Schumann, C. Rieder, J. Bieberstein, A. Weihusen, S. Zidowitz, J.-H. Moltz, and T. Preusser. State of the art in computer-assisted planning, intervention and assessment of liver tumor ablation. In *Critical Reviews^{TM} in Biomedical Engineering (Special Issue on Thermal Tumor Ablation)*, volume 38, pages 31–52, 50 Cross Highway 50 Cross Highway, Redding, CT 06896, 2010. begell house, inc.

[29] U. Tiede, T. Schiemann, and K. Hohne. High quality rendering of attributed volume data. *Visualization '98. Proceedings*, pages 255 – 262, 1998.

[30] C. Tietjen, B. Meyer, S. Schlechtweg, B. Preim, I. Hertel, and G. Strauß. Enhancing slice-based visualizations of medical volume data. *IEEE/Eurographics Symposium on Visualization (EuroVis)*, pages 123–130, 2006.

[31] K. Trovato, S. Dalal, J. Krcker, A. Venkatesan, and B. J. Wood. Automated rfa planning for complete coverage of large tumors. In *Proc SPIE Medical Imaging*, volume 7261, pages 72610D.1–72610D.7, 2009.

[32] C. Villard, L. Soler, and A. Gangi. Radiofrequency ablation of hepatic tumors: simulation, planning, and contribution of virtual reality and haptics. *Comp. Methods in Biomechanics & Biomedical Eng.*, 8(4):215–227, 2005.

[33] C. Villard, L. Soler, N. Papier, V. Agnus, S. Thery, A. Gangi, D. Mutter, and J. Marescaux. Virtual radiofrequency ablation of liver tumors, Jan 2003.

[34] A. Weihusen, L. Hinrichsen, T. Carus, R. Dammer, R. Rascher-Friesenhausen, T. Kröger, H. Peitgen, and T. Preusser. Towards a verified simulation model for radiofrequency ablations. *Information Processing in Computer-Assisted Interventions*, pages 179–189, 2010.

[35] A. Weihusen, F. Ritter, T. Kröger, T. Preusser, S. Zidowitz, and H.-O. Peitgen. Workflow oriented software support for image guided radiofrequency ablation of focal liver malignancies. *Proceedings of SPIE*, Jan 2007.

[36] W. Zhai, J. Xu, Y. Zhao, Y. Song, L. Sheng, and P. Jia. Preoperative surgery planning for percutaneous hepatic microwave ablation. *MICCAI*, (LNCS 5242):569–577, Jul 2008.

[37] S. Zidowitz, H. Drexl, T. Kröger, T. Preusser, F. Ritter, A. Weihusen, and H.-O. Peitgen. Baysian Vessel Extraction for Planning of RF-Ablation. *Bildverarbeitung für die Medizin*, pages 187–191, 2007.